

Nonequilibrium Multiple Transitions in the Core-shell Ising Nanoparticles Driven by Randomly Varying Magnetic Fields

Erol Vatansever^{1,*} and Muktish Acharyya^{2,†}

¹*Department of Physics, Dokuz Eylul University, TR-35160, Izmir-Turkey*

²*Department of Physics, Presidency University, 86/1 College Street, Kolkata-700073, India*

E-mail*:erol.vatansever@deu.edu.tr

E-mail†:muktish.physics@presiuniv.ac.in

Abstract: The nonequilibrium behaviour of a core-shell nanoparticle has been studied by Monte-Carlo simulation. The core consists of Ising spins of $\sigma = 1/2$ and the shell contains Ising spins of $S = 1$. The interactions within the core and in the shell are considered ferromagnetic but the interfacial interaction between core and shell is antiferromagnetic. The nanoparticle system is kept in open boundary conditions and is driven by randomly varying (in time but uniform over the space) magnetic field. Depending on the width of the randomly varying field and the temperature of the system, the core, shell and total magnetization varies in such a manner that the time averages vanish for higher magnitude of the width of random field, exhibiting a dynamical symmetry breaking transitions. The susceptibilities get peaked at two different temperatures indicating nonequilibrium multiple transitions. The phase boundaries of the nonequilibrium multiple transitions are drawn in the plane formed by the axes of temperature and the width of the randomly varying field. Furthermore, the effects of the core and shell thicknesses on the multiple transitions have been discussed.

Keywords: Magnetic hyperthermia, Core/shell nanoparticles, Monte Carlo simulation, Dynamic phase transitions

1 Introduction

The random field Ising model (RFIM) including quenched random magnetic field has attracted a considerable interest in the last four decades [1, 2]. Despite of its simplicity, many problems in statistical physics and condensed matter physics can be studied by means of RFIM. Experimental examples include diluted antiferromagnets $\text{Fe}_x\text{Zn}_{1-x}\text{F}_2$ [3, 4], $\text{Rb}_2\text{Co}_x\text{Mg}_{1-x}\text{F}_4$ [5, 6], $\text{Co}_x\text{Zn}_{1-x}\text{F}_2$ [6] in a magnetic field and colloid-polymer mixtures [7, 8]. From the theoretical point of view, thermal and magnetic phase transition properties of the static RFIM have been investigated by a wide variety of techniques such as Molecular Field Theory (MFT) [2, 9–13], Effective-Field Theory (EFT) [14–20] and Monte Carlo (MC) simulations [21–28]. These theoretical studies show that different random-field distributions may lead to different physical outcomes, and thereby the existence of a quenched impurity in magnetic field has an important role in material science. They also indicate that our understanding of equilibrium critical phenomena associated with the RFIM has reached a point in which the satisfactory results are available. The readers may refer to [29] for a detailed review of recent developments in the RFIM. However, far less is known for the physical mechanisms underlying the out of equilibrium phase transitions of the Ising systems in the presence of a randomly varying magnetic field.

Stationary state properties of a randomly driven Ising ferromagnet has been investigated by benefiting from the Glauber dynamics [30]. Based on the MFT calculations, it is found that the system shows a first-order phase transition related to dynamic freezing. Paula and Figueiredo [31] have attempted to study dynamical behavior of the Ising model in a quenched random magnetic field, with a bimodal distribution for the random fields. The dynamics of the system has been defined in terms of Glauber type stochastic process. It is obtained that the magnetic field values leading to first-order transitions are greater than the corresponding fields at equilibrium. One of us [32] has focused on the two dimensional Ising model in the presence of randomly varying magnetic field to understand how the randomly changing magnetic affects the physical properties of the system. By benefiting from both MFT and MC simulations, it is reported that the time-averaged magnetization disappears from a nonzero value depending upon the values of the width of randomly varying field and the temperature. Nonequilibrium phase transition properties in a three-dimensional lattice system with random-flip kinetics have been elucidated in detail by using MC simulations [33]. One of the remarkable findings is that the system displays a first-order phase transitions located at low temperature region and large disorder strengths, denoting a nonequilibrium tri-critical point at a finite temperature. Moreover, nonequilibrium phase transitions and stationary-state solutions of a three-dimensional random-field Ising model under a time-dependent periodic external field have been investigated within the framework of EFT with single-site correlations [34]. The amplitude of the external is chosen such that they will be according to bimodal and trimodal distribution functions. It is shown that the system explicit unusual and interesting behaviors depending on type of the magnetic field source. The readers may refer to [35] for a review of the dynamic phase transitions and hysteresis phenomena observed in different kinds of magnetic systems. To the best our knowledge, all of the studies mentioned above have been dedicated to bulk materials in the presence of randomly varying magnetic field. There are, however, only a few studies regarding the random magnetic field effects on the core/shell nanoparticle systems including surface and finite size effects [36–38]. It is a well known fact that when the physical size of an interacting magnetic system reduces to a characteristic length, surface effects begin to show themselves on the system, and as a result of this, some interesting behaviours can be observed, differing from those of bulk systems [39]. Two notable examples are Co/CoO [40, 41]

and Mn/Mn₃O₄ [42], where the physical properties of the nanoparticles sensitively depend on its own chemical characters. In this paper, we will consider the core/shell ferrimagnetic nanoparticle system driven by a randomly varying magnetic field. More specifically, our motivation is to understand how randomly changing field affects the thermal and magnetic properties of a nanoparticle, by means of an extensive MC simulation. In a nutshell, our simulation results indicate that the present system exhibits multiple dynamic phase transitions depending on the chosen values of the external magnetic field width and the temperature of the system.

The rest of the paper is organized as follows: In Sec. (2), we present the model and simulation details. The numerical findings and discussion are given in Sec. (3), finally Sec. (4) is dedicated to a brief summary of our conclusion.

2 Model and Simulation Details

We consider a cubic with thickness ($L = L_c + L_{sh}$) ferrimagnetic nanoparticle composed of a spin-1/2 ferromagnetic core which is surrounded by a spin-1 ferromagnetic shell layer. Here, L , L_c and L_{sh} are the total, core and shell thicknesses of the particle, respectively. At the interface, we define an antiferromagnetic interaction between core and shell spins. The nanoparticle is exposed to a time dependent randomly varying magnetic field. The Hamiltonian describing our system can be written as follows:

$$H = -J_c \sum_{\langle ij \rangle} \sigma_i \sigma_j - J_{sh} \sum_{\langle kl \rangle} S_k S_l - J_{int} \sum_{\langle ik \rangle} \sigma_i S_k - h(t) \left(\sum_i \sigma_i + \sum_k S_k \right) \quad (1)$$

here $\sigma_i = \pm 1/2$ and $S_k = \pm 1, 0$ are spin variables corresponding to the core and shell parts of the particle, respectively. J_c and J_{sh} denotes the ferromagnetic spin-spin interactions in the core and shell components of the system while J_{int} is the antiferromagnetic interaction at the interface of the particle. The symbol $\langle \dots \rangle$ represents the nearest neighbor interactions in the system. $h(t)$ is the randomly varying magnetic field (in time but uniform in space). The time variation of $h(t)$ can be given as follows [32]:

$$h(t) = \begin{cases} h_0 r(t) & \text{for } t_0 < t < t_0 + \tau \\ 0 & \text{otherwise} \end{cases} \quad (2)$$

where $r(t)$ is the random number which is distributed uniformly between -1/2 and 1/2. Thereby, the field $h(t)$ varies randomly from $-h_0/2$ to $h_0/2$ and,

$$\frac{1}{\tau} \int_{t_0}^{t_0+\tau} h(t) dt = 0 \quad (3)$$

For the sake of simplicity, J_{sh} is fixed to unity throughout the simulations, and the remaining system parameters are normalized with J_{sh} . In order to study thermal and magnetic properties of the system, we employ Monte Carlo simulation with single-site update Metropolis algorithm [43,44] on a $L \times L \times L$ simple cubic lattice. We apply boundary conditions such that they are free in all directions of the particle. We note that such type of a boundary condition is an appropriate choice for considered finite small system. Let us briefly summarize the simulation protocol we follow here: The system is in contact with an isothermal heat bath at a reduced temperature $k_B T / J_{sh}$, where k_B is the Boltzmann constant. Spin configurations were produced by selecting the spins randomly

through the lattice, and the single-site update Metropolis algorithm was used for each considered spin. This process was repeated L^3 times, which also defines a MC step per site.

Using the above scheme we simulated the nanoparticle system. 100 independent initial configurations have been generated to get a satisfactory statistics. For each initial spin configuration, the first 5×10^5 MC steps have been discarded for thermalization process, and the numerical data were measured during the following 5×10^5 MC steps. Based on our detailed test calculations, it is possible to say that this number of transient steps is found to be enough for thermalization of the particle. We have verified that higher values of transient steps does not change the outcomes reported here. Error bars have been obtained using the jackknife method [43]. The main quantity of interest is the time-averaged magnetization, which is defined as follows:

$$Q_\alpha = \frac{1}{\tau} \int_{t_0}^{t_0+\tau} m_\alpha(t) dt \quad (4)$$

where $\alpha = c, sh$ and T corresponding to the core and shell components of the particle and the overall of the system. $m_\alpha(t)$ is the time-dependent magnetization, which can be given as follows:

$$m_c(t) = \frac{1}{N_c} \sum_i^{N_c} \sigma_i, \quad m_{sh}(t) = \frac{1}{N_{sh}} \sum_i^{N_{sh}} S_i, \quad m_T(t) = \frac{N_c m_c(t) + N_{sh} m_{sh}(t)}{N_c + N_{sh}} \quad (5)$$

here $N_c = L_c^3$ and $N_{sh} = L^3 - L_c^3$ denotes the total number of spins lying in the core and shell parts of the system, respectively. We select the number of core and shell spins as $N_c = 10^3$ and $N_{sh} = 14^3 - 10^3$, such that it allows us to create a core-shell nanocubic particle with shell thickness $L_{sh} = 2$ unless otherwise stated. We also define two additional order parameters for the core and shell layers of the particle as follows:

$$O_c = \frac{N_c}{N_c + N_{sh}} Q_c, \quad O_{sh} = \frac{N_c}{N_c + N_{sh}} Q_{sh}. \quad (6)$$

By benefiting from the definitions given in Eq. (6), the total order parameter can be defined by: $O_T = O_c + O_{sh}$. To estimate the pseudo-critical transition temperature for a finite-size system as a function of the external field, it is useful to focus on the scaled variances of the dynamic order parameters [45],

$$\chi_\alpha = N_\alpha (\langle O_\alpha^2 \rangle - \langle |O_\alpha| \rangle^2), \quad (7)$$

where $N_T = N_c + N_{sh}$ is the total number of spins in the system. In addition to the Eq. (7), we also measure the scaled variance of the total energy (which can be considered as heat-capacity in equilibrium system) of the particle including the cooperative part as follows:

$$\chi_E = N_T (\langle E^2 \rangle - \langle E \rangle^2), \quad (8)$$

where E is the time-averaged energy of the particle per site, which is defined as follows:

$$E = -\frac{1}{\tau N_T} \int_{t_0}^{t_0+\tau} \left[J_c \sum_{\langle ij \rangle} \sigma_i \sigma_j + J_{sh} \sum_{\langle kl \rangle} S_k S_l + J_{int} \sum_{\langle ik \rangle} \sigma_i S_k \right] dt. \quad (9)$$

3 Results and discussion

Figure 1 shows the time series of core $m_c(t)$, shell $m_{sh}(t)$ and total $m_T(t)$ magnetizations at a considered value of temperature and for two different values of randomly field width h/J_{sh} . All numerical results given here are obtained for $k_B T/J_{sh} = 2.0$. It is clear from the Figure 1(a) that when the external field width is relatively small (for example $h/J_{sh} = 1.0$) time dependent magnetizations can not give a response to changing magnetic field simultaneously. Thereby, the system remains in a dynamically symmetry broken phase where the instantaneous magnetizations oscillate around a non-zero value. If h/J_{sh} gets bigger, time dependent magnetizations tend to give an answer to randomly changing magnetic field. Therefore, the system remains in a dynamically symmetric phase where the magnetizations oscillate around zero value, as depicted in Figure 1(b). The results aforementioned here indicate that dynamics of the core/shell nanoparticle sensitively depends on the chosen external field width value. It should be noted that such type of an observation has been reported for the bulk spin-1/2 Ising models driven by a randomly changing magnetic field in both two and three-dimensional space [32,34].

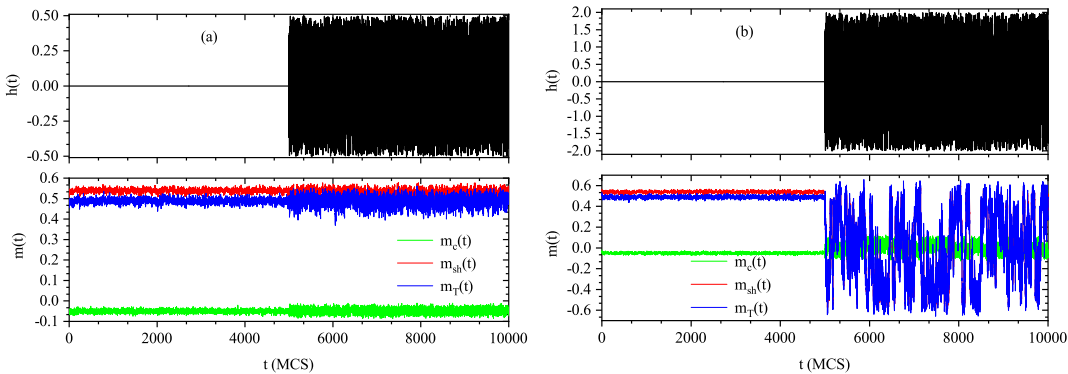


Figure 1: (Color online) Monte Carlo results of the time variations of randomly changing magnetic field and core, shell and total magnetizations. All results are obtained for a fixed temperature $k_B T/J_{sh} = 2.0$ and the chosen values of the spin-spin couplings $J_c/J_{sh} = 0.75$ and $J_{int}/J_{sh} = -1.5$. Magnetic field sources, (a) $h/J_{sh} = 1.0$ and (b) $h/J_{sh} = 4.0$, are opened at $t = 5000$ MCs. This diagram demonstrates the dynamical symmetry breaking associated to the transition.

As displayed in Figure 2, in order to get a better understanding of the effect of randomly varying magnetic field width on the critical properties of the considered nanoparticle, we present the dynamic phase diagram plotted in a $(h/J_{sh} - k_B T_C/J_{sh})$ plane for a selected combination of system parameters such as $J_{int}/J_{sh} = -1.5$ and $J_c/J_{sh} = 0.75$. Here, T_C means the pseudo-critical temperature. Transition temperatures are extracted from the thermal variations of variances of the core, shell and total dynamic order parameters and internal energies. One of the outstanding results is that there is a multiple phase transition region including two branches in the system up to a particular magnetic field width. In this region, when the temperature increases starting from the relatively lower values, it has been found that the core magnetization first exhibits a phase transition. This corresponds to the first branch of the multiple transition line. Furthermore, if the temperature is increased further, then the overall particle shows a transition between ordered and disordered phases for a fixed value of h/J_{sh} . Such kind of a transition corresponds to the second branch of multiple transition line. Our Monte Carlo simulation findings show that the multiple transitions observed here strongly depend on the chosen applied field width value. As explicitly seen from the phase diagram, transition temperatures decrease when the h/J_{sh} value gets bigger.

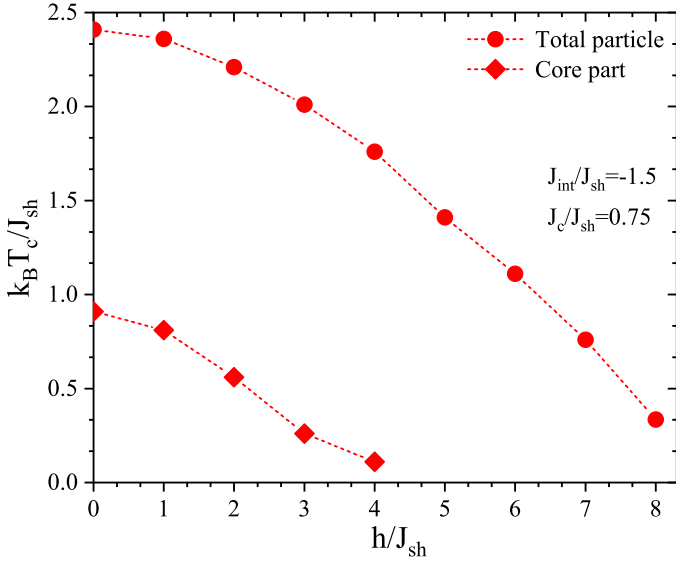


Figure 2: (Color online) Dynamic phase boundary of core-shell nanocubic system in a $(h/J_{sh} - k_B T_c/J_{sh})$ plane for selected values of $J_c/J_{sh} = 0.75$ and $J_{int}/J_{sh} = -1.5$. The magnetic field varies randomly between $-h/2J_{sh}$ and $h/2J_{sh}$. Transition points are obtained from the peak positions of the variances of the core, shell and total magnetizations and specific heat curve of the nanoparticle as a function of temperature.

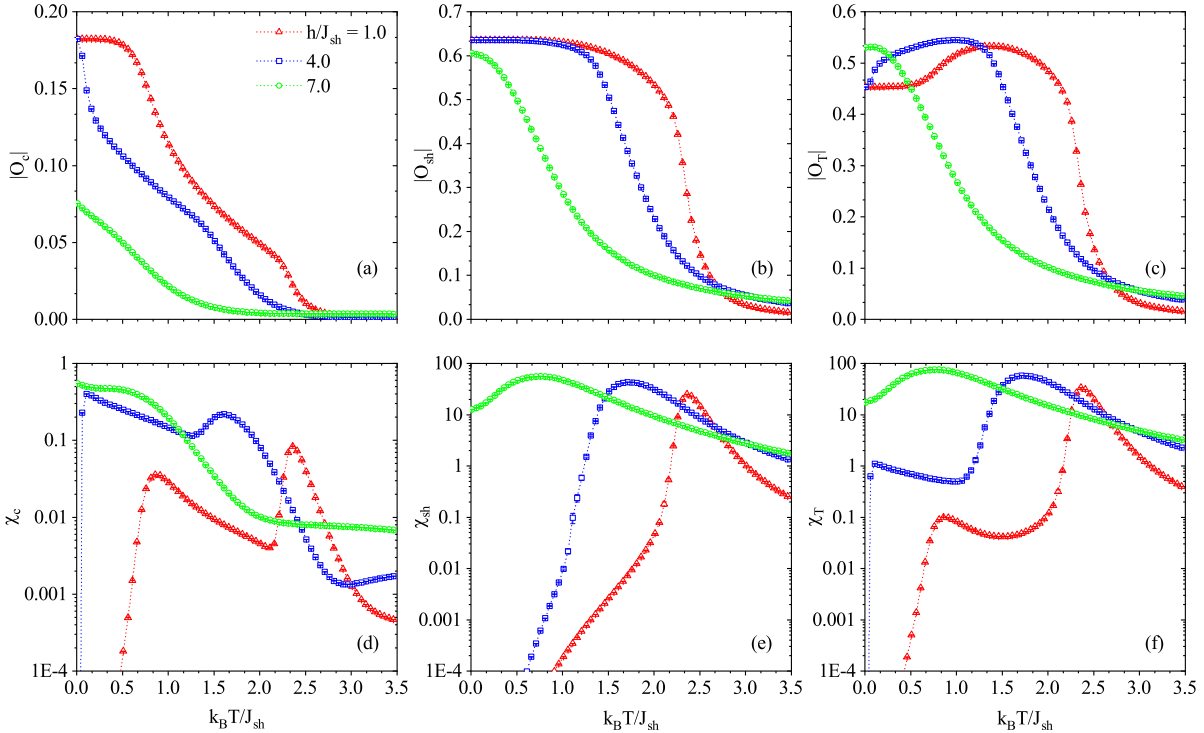


Figure 3: (Color online) Effects of the randomly changing magnetic field width on the core (a), shell (b) and the total magnetizations (c), and their corresponding variances (d), (e) and (f), respectively. Here, different symbols denote the varying magnetic values.

This is because the energy contribution coming from the Zeeman term to the total energy increases with an increment in h/J_{sh} . Thereby, the phase transition lines get shrink. We note that all of the transitions found here are second-order transition, i.e., there is no first-order phase transition in the system, indicating a tri-critical point where the first-order transition lines are met with the second-order transition lines. Similar kind of a multiple transition has also been reported in Ref. [46] where thermal and magnetic properties of a classical anisotropic Heisenberg model driven by a polarized magnetic field are investigated by means of MC simulations.

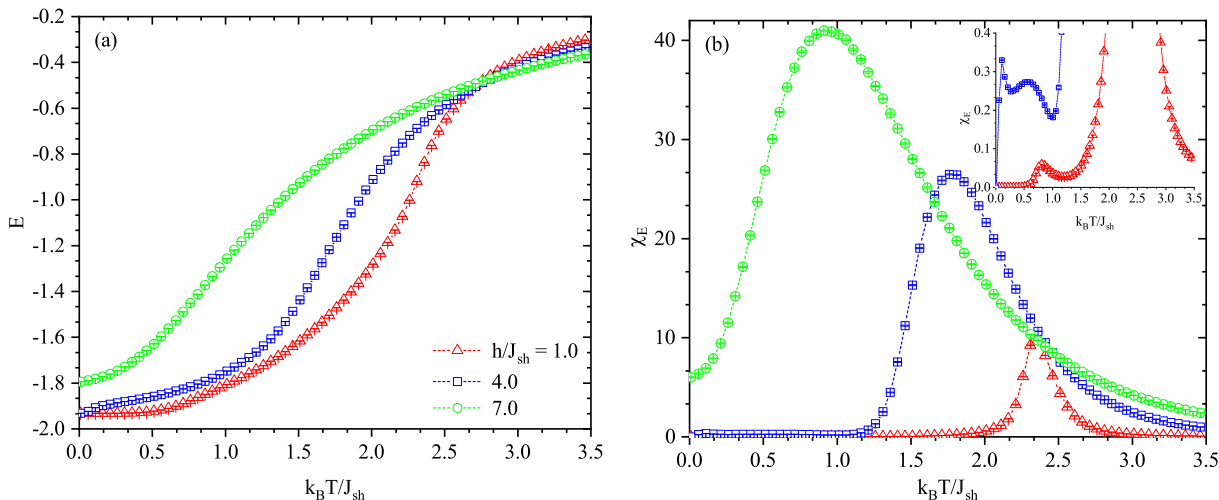


Figure 4: (Color online) Thermal variations of the internal energy (a) and the corresponding variances (b). The curves are obtained for three different values of the randomly changing magnetic field: $h/J_{sh} = 1.0, 4.0$ and 7.0 . Inset given here represents the low temperature regions of the variances of the internal energies for two considered values of h/J_{sh} : 1.0 and 4.0 .

In Figures 3(a-c), we depict the effect of randomly changing magnetic field width on the core, shell and total dynamic order parameters as functions of the temperature, corresponding to the dynamic phase diagram given in Figure 2. As an interesting observation, we can see from total magnetization curves plotted in Figure 3(c), they exhibit a temperature induced maximum, which is strongly depend on the chosen applied field width. At this point we note that in the bulk ferrimagnetism of Néel [47,48], it is possible to classify the magnetization profiles based on the total magnetization behaviors in certain categories. According to this nomenclature, the system shows a P-type behavior for some selected values of h/J_{sh} such as 1.0 and 4.0 . It also means that the results given here are in common at various types of magnetic materials, which are not only dependent on their size. As the h/J_{sh} gets bigger, for example $h/J_{sh} = 7.0$, P-type behavior observed here tends to disappear, leading to a Q-type behavior. In Figures 3(d-f), we present the thermal variations of the variances of core, shell and total dynamic order parameters for the same system parameters used in Figures 3(a-c). As clearly seen from the figures that when the temperature reaches to the transition temperature, the related variances give rise to show a peak behavior, which is also a fingerprint of a continuous transition. Peak positions in x -axis are sensitively dependent on the studied external field width such that they tend to decrease with an increment in h/J_{sh} . Moreover, it is obvious from the Figure 3(d) that the variance of core magnetization shows two peaks for some selected values of h/J_{sh} such as 1.0 and 4.0 . The first peak located at the relatively lower temperature region originates from the order-disorder transition of the core part of the nanoparticle whereas the second one is a result of the strong

coupling between core and shell layers.

In Figure 4, we give the thermal variations of the internal energy and corresponding variances for the same applied field width values used in Figure 3. When the temperature begins to decrease starting relatively higher values, numerical values of the internal energies are decreased for all values of h/J_{sh} . In addition to this general trend, as shown in Figure 4(a), it is possible to say that a sudden decrement is observed when the temperature reaches to the relevant critical point, as in the case of equilibrium phase transitions [43, 44]. More specifically, figure 4(b) displays the variances of the internal energies as functions of the temperatures. As in the case of the variances of the dynamic order parameters discussed above, when the temperature reaches to the critical point, they tend to show a clear peak behavior, indicating a second-order phase transition. Their positions on the x -axis are sensitively dependent on the considered applied field width values. In accordance with the previously observed results from the variances of the dynamic order parameters, the pseudo-critical temperatures start to shift to the lower regions with increasing h/J_{sh} values. In the inset, we also plot the low temperature behavior of the χ_E for two considered applied field width h/J_{sh} such as 1.0 and 4.0. It is clear from the figure that, it shows a clear peak treatment supporting the transition of the nanoparticle belonging to only the core part, in the vicinity of the related transition point.

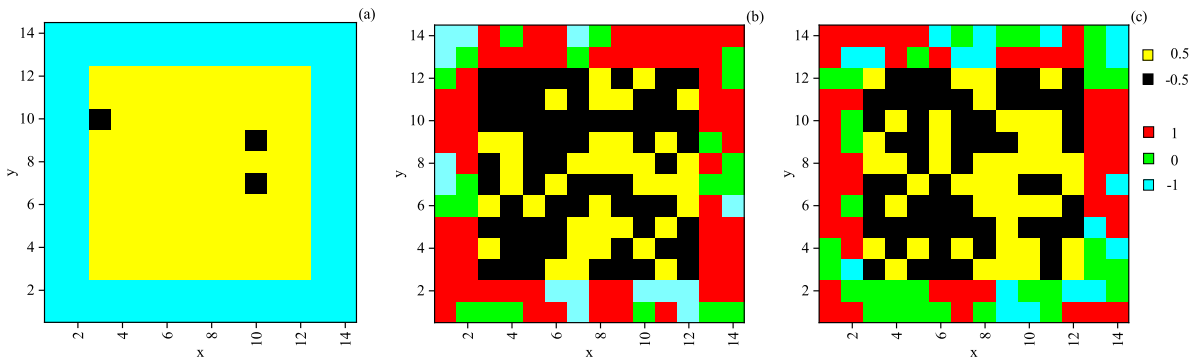


Figure 5: (Color online) The spin configurations of the midplane cross-sections of the nanoparticle in the $x - y$ plane. They are taken for three different temperature values: (a) $k_B T / J_{sh} = 0.5$ (ordered region), (b) 2.36 (in the vicinity of transition point) and (c) 4.0 (disordered region) with $h / J_{sh} = 1.0$. All snapshots are captured at $t = 75 \times 10^4$ MCs. Here, yellow, black, red, green and cyan colors correspond to the spin values of 0.5, -0.5 , 1, 0 and -1 , respectively.

We represent the spin configurations of the midplane cross-sections of the nanoparticle in the $x - y$ plane in Figure 5. All snapshots are captured for the $h / J_{sh} = 1.0$. By benefiting from the calculations mentioned above, the pseudo-critical is obtained as $k_B T_C / J_{sh} \approx 2.36$ for $h / J_{sh} = 1.0$. In order to show the influences of the temperature on the spin-snapshots, three different temperature values are taken into consideration, being smaller (a), equal (b) and larger than the critical temperature. As seen clearly from the figure 5(a) that the spins in the core and shell parts of the system are opposite to each other due the existence of an antiferromagnetic exchange coupling between core and shell layers of the nanoparticle. However, when taking a look at the core and shell layers of the system one by one, it is seen that most of the spins in related layers are aligned parallel to each other, causing to an ordered phase. When the temperature reaches to the critical temperature, strong fluctuations take place in the nanoparticle, as depicted in Figure 5(b). On the other hand, above $k_B T_C / J_{sh}$, the spins in the system try to follow randomly changing magnetic field. Therefore, they are aligned with respect to each other almost randomly

[see Figure 5(c)].

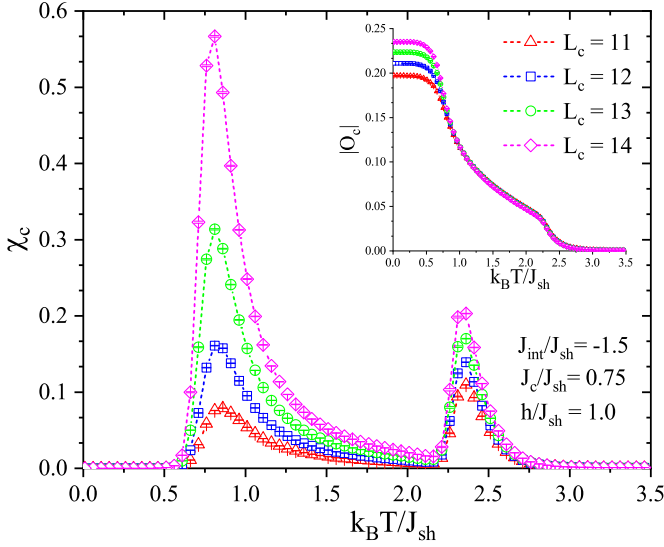


Figure 6: (Color online) Thermal variations of the core susceptibilities for considered values of the system parameters such as $J_{int}/J_{sh} = -1.5$, $J_c/J_{sh} = 0.75$, $h/J_{sh} = 1.0$ and $L_{sh} = 2$. The curves are plotted for four values of the core thickness: $L_c = 11, 12, 13$ and 14 . The inset represents the temperature dependencies of the core magnetizations for the same parameter set used for the core susceptibilities curves.

Figure 6 displays the influences of core thickness on the core susceptibilities (main panel) and the core magnetizations (inset) for considered values of the system parameters such as $J_{int}/J_{sh} = -1.5$, $J_c/J_{sh} = 0.75$, $h/J_{sh} = 1.0$ and $L_{sh} = 2$. The curves are obtained for four values of $L_c = 11, 12, 13$ and 14 . It can be deduced from the figure that the multiple transition behavior is not affected by the variation of the core thickness. When L_c gets bigger, the height of the core susceptibilities even prominently increases, leading to a strong ferromagnetic character in the core part of the nanoparticle. The behavior mentioned here is also seen in the curves of the core magnetization as a function of the temperature. Although all curves qualitatively are similar to each other, the saturation values sensitively depend on the chosen value of L_c . Moreover, in order to see whether the multiple phase transition character obtained here depends on the sign of the interface coupling parameter or does not, we give again the core susceptibilities (main panel) and core magnetizations (inset) versus temperature curves, as displayed in Figure 7. We changed only the sign of the J_{int}/J_{sh} parameter without changing its magnitude for the same system parameters used for Figure 6 with $L_c = 10$. It is clear from the figure that thermal variations of the core susceptibilities show a double-peak behavior, and the phase transition temperatures corresponding to the core part and overall nanoparticle are almost the same for both values of $J_{int}/J_{sh} = 1.5$ and -1.5 . The inset displays the thermal variations of the core magnetizations for the same parameter set. We note that there is a clear agreement between these two curves obtained for the values of $J_{int}/J_{sh} = 1.5$ and -1.5 . We also checked the remaining quantities such as the shell and the total order parameters, corresponding susceptibilities, the internal energies and the specific heat curves as functions of the temperature, which are not given here, and almost the same results have been obtained for both values of J_{int}/J_{sh} . In view of all these observations, we can say that a variation in the sign of the interface coupling, $J_{int}/J_{sh} \rightarrow -J_{int}/J_{sh}$, does not significantly affect the multiple transition behavior reported here. We note that such kind of studies considering the

effects of the sign of the interface coupling parameter on the magnetic properties of the different kinds of core/shell nanoparticle systems have been elucidated in the references [49, 50].

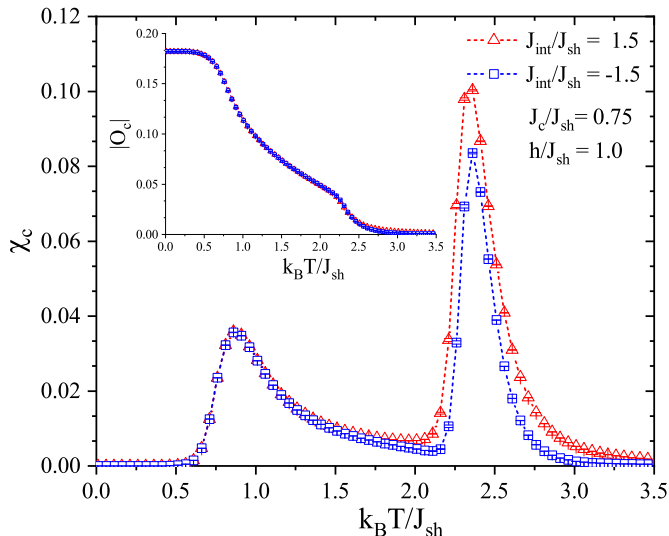


Figure 7: (Color online) Monte Carlo simulation results of the thermal variations of core susceptibilities of the nanoparticle for varying values of J_{int}/J_{sh} . All results are obtained for some selected values of the system parameters such as $h/J_{sh} = 1.0$, $J_c/J_{sh} = 0.75$, $L_{sh} = 2$ and $L_c = 10$. The corresponding core parts of the nanoparticle for the same parameter set are displayed in the inset.

As a final investigation, in order to show the effects of the varying system size of the nanoparticle on its thermal and magnetic properties, we depict the dynamic phase boundary in a $(L_{sh} - k_B T_c / J_{sh})$ plane in Figure 8(a) for considered values of the system parameters: $J_{int}/J_{sh} = -1.5$, $J_c/J_{sh} = 0.75$ and $h/J_{sh} = 1.0$. We followed the same way mentioned above to extract the phase transition points. It is worthwhile to mention that there is still a multiple phase transition behavior including two branches in the system for all selected values of L_{sh} . More specifically, the phase transition point regarding the overall nanoparticle tends to increase with increasing L_{sh} starting from $L_{sh} = 2$, and it saturates to a certain value with further increment in L_{sh} . It means that after a certain value of L_{sh} the boundary conditions begin to lose its effect on the system, and the systems starts to behave like a bulk system. It should be noted that varying shell thickness values do not affect the first branch of the phase diagram where the core magnetization shows a phase transition, in accordance with the expectations. In other words, the critical temperature for core part of the nanoparticle is insensitive to the shell thickness of the system. As seen in Figures 8(b) and (c), varying shell thickness values affect clearly the core, shell and total magnetizations of the system. The saturation value of the shell magnetization increases when L_{sh} gets bigger. Another important findings is that the total magnetization as a function of the temperature starts to evolve from the P-type to Q-type behavior with increasing L_{sh} [48].

4 Concluding Remarks

The equilibrium behaviours of the core-shell nanoparticles have been investigated widely and well understood. However, the nonequilibrium responses of the core-shell nanoparticles have not yet been investigated. Here we have studied the nonequilibrium responses of Ising core-shell nanoparticles driven by randomly varying (in time but uniform over the space) magnetic field. The time

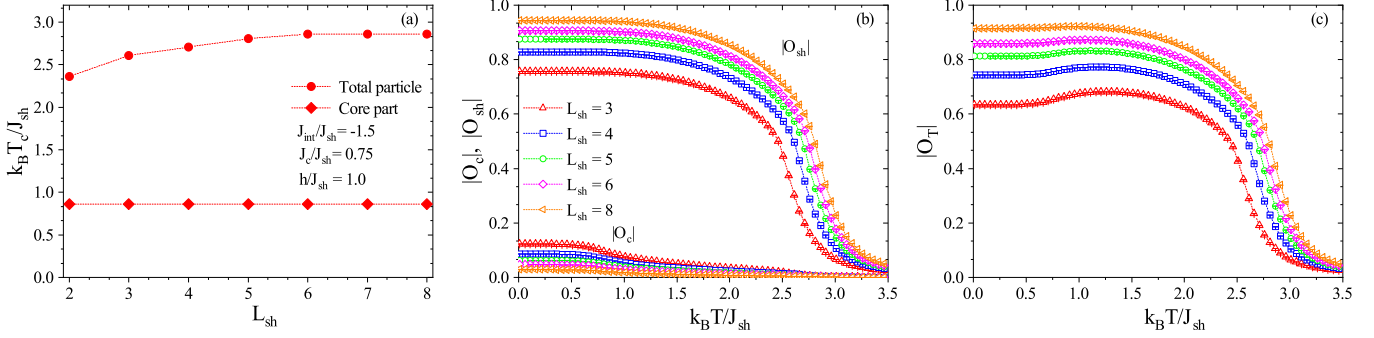


Figure 8: (Color online) (a) Shell thickness dependencies of the dynamic critical points of a cubic core/shell nanoparticle for considered values of the system parameters such as $J_{int}/J_{sh} = -1.5$, $J_c/J_{sh} = 0.75$ and $h/J_{sh} = 1.0$. The effects of the shell thickness on the thermal variations of core and shell (b) and total (c) magnetizations at varying values of the shell thickness $L_{sh} = 3, 4, 5, 6$ and 8.

dependent magnetic field keeps the core-shell nanoparticle far from equilibrium. Hence, the responses of the system is truly of nonequilibrium type. The ferromagnetic Ising (spin-1/2) core is covered by ferromagnetic Ising (spin-1) shell. However, the interfacial interaction between core and shell is being considered as antiferromagnetic. We have calculated the time averaged core magnetization, shell magnetization and the total magnetization and their variances (susceptibility in a sense) and studied those as functions of the temperature with field as parameter. We have observed, for relatively higher value of the temperature and the width of the randomly varying magnetic field, the system shows a dynamical symmetric behaviour. In this case, the instantaneous magnetizations are found to fluctuate symmetrically around zero value. On the other hand, for relatively lower values of the temperature and the field width a dynamically symmetry broken phase is observed. Where the instantaneous magnetizations fluctuates asymmetrically around zero value. These are demonstrated in figure-1. Obviously, a nonequilibrium phase transition is observed in association with a dynamical symmetry breaking although the concept of symmetry breaking was originally made for the system in thermodynamic limit. In the above mentioned dynamically symmetric phase, the time averaged magnetizations (serving as the order parameters in the present study) vanishes, indicating a nonequilibrium disordered phase. Whereas, in the dynamically asymmetric phase, the time averaged magnetizations, acquires nonzero values, indicating the nonequilibrium ordered phase. The transition temperatures were estimated from the value of the temperatures where the variances of those magnetizations get peaked (believed to be diverging in the thermodynamic limit). It was observed, that the variance of total magnetization gets peaked at higher temperature and that of core magnetization gets peaked at some lower temperature. This is a signature of *nonequilibrium multiple phase transition* observed in the driven core-shell nanoparticle.

Collecting all these nonequilibrium transition temperatures the comprehensive nonequilibrium phase diagram is drawn in the plane consists with the axes of the temperature and the width of the randomly varying magnetic field.

It would be quite interesting to study such behaviours in the case of Ising core-shell nanoparticles where the values, of spins in the core and that in the shell, differs largely. That will affect certainly on the difference in the region bounded by core-transition line and the shell-transition line in the comprehensive phase diagram. What will be the effects of dilution here? If the core

and shell are diluted by nonmagnetic impurities (with different concentrations in core and shell), how does it affect the phase boundaries of the multiple phase diagram. Last but not the least, how sensitive the nature of the distribution (i.e., uniform, bimodal, normal) of the randomly varying magnetic fields, would also be an interesting matter to be studied. We have plans to study these and the results will be reported elsewhere.

Acknowledgements

The numerical calculations reported in this paper were performed at TUBITAK ULAKBIM High Performance and Grid Computing Center (TR-Grid e-Infrastructure). MA acknowledges FRPDF research grant provided by Presidency University.

References

- [1] Y. Imry, S.-K. Ma, Phys. Rev. Lett. **35**, 1399 (1975).
- [2] A. Ahorony, Phys. Rev. B **18**, 3318 (1978).
- [3] D.P. Belanger, A.R. King, V. Jaccarino, Phys. Rev. B **31**, 4538 (1985).
- [4] A.R. King, V. Jaccarino, D.P. Belanger, S.M. Rezende, Phys. Rev B **32**, 503 (1985).
- [5] I.B. Ferreira, A.R. King, V. Jaccarino, J.L. Cardy, H.J. Guggenheim, Phys. Rev. B **28**, 5192 (1983).
- [6] H. Yoshizawa, R.A. Cowley, G. Shirane, R.J. Birgeneau, H.J. Guggenheim, H. Ikeda, Phys. Rev. Lett. **48**, 438 (1982).
- [7] R.L.C. Vink, K. Binder, H. Löwen, Phys. Rev. Lett. **97**, 230603 (2006).
- [8] M.A. Annunziata, A. Pelissetto, Phys. Rev. E **86**, 041804 (2012).
- [9] T. Schneider, E. Pytte, Phys. Rev. B **15**, 1519 (1977).
- [10] D. Andelman, Phys. Rev. B **27**, 3079 (1983).
- [11] D.C. Mattis, Phys. Rev. Lett. **55**, 3009 (1985).
- [12] M. Kaufman, P.E. Klunzinger, A. Khurana, Phys. Rev. B **34**, 4766 (1986).
- [13] S.M.D. Queirós, N. Crokidakis, D.O.S.-Pinto, Phys. Rev. E **80**, 011143 (2009).
- [14] H.E. Borges, P.R. Silva, Physica A, **144**, 561 (1987).
- [15] E.F. Sarmiento, T. Kaneyoshi, Phys. Rev. B **39**, 9555 (1989).
- [16] R.M. Sebastianes, W. Figueiredo, Phys. Rev. B **46**, 969 (1992).
- [17] T. Kaneyoshi, Physica A, **139**, 455 (1986).
- [18] D.F. Albuquerque, I.P. Fittipaldi, J.R. de Sousa, N.O. Moreno, Physica B **384**, 230 (2006).

- [19] Ü. Akinci, Y. Yüksel, H. Polat, Phys. Rev. E **83**, 061103 (2011).
- [20] G. Karakoyun, Ü. Akinci, Physica B **578**, 411870 (2020).
- [21] D.P. Landau, H.H. Lee, W. Kao, J. Appl. Phys. **49**, 1356 (1978).
- [22] J. Machta, M.E.J. Newman, L.B. Chayes, Phys. Rev. E **62**, 8782 (2000).
- [23] N.G. Fytas, A. Malakis, K. Eftaxias, J. Stat. Mech. **P03015** (2008).
- [24] N.G. Fytas, A. Malakis, Eur. Phys. J. B **61**, 111 (2008).
- [25] M. Gofman, J. Adler, A. Ahorony, A.B. Harris, M. Schwartz, Phys. Rev. B **53**, 6362 (1996).
- [26] N.G. Fytas, V.M.- Mayor, G. Parisi, M. Picco, N. Surlas, J. Stat. Mech. **093203** (2019).
- [27] N.G. Fytas, V.M.- Mayor, G. Parisi, M. Picco, N. Surlas, Phys. Rev. Lett. **122**, 240603 (2019).
- [28] N.G. Fytas, V.M.- Mayor, M. Picco, N. Surlas, Phys. Rev. E **95**, 042117 (2017).
- [29] N.G. Fytas, V.M.- Mayor, M. Picco, N. Surlas, J. Stat. Phys. **172**, 665 (2018).
- [30] J. Hausmann, P. Ruján, Phys. Rev. Lett. **79**, 3339 (1997).
- [31] G.L.S. Paula, W. Figueiredo, Eur. Phys. J. B **1**, 519 (1998).
- [32] M. Acharyya, Phys. Rev. E **58**, 174 (1998).
- [33] N. Crokidakis, Phys. Rev. E **81**, 041138 (2010).
- [34] Y. Yüksel, E. Vatansever, Ü. Akinci, H. Polat, Phys. Rev. E **85**, 051123 (2012).
- [35] B.K. Chakrabarti, M. Acharyya, Rev. Mod. Phys. **71**, 847 (1999).
- [36] A. Zaim, M. Kerouad, M. Boughrara, EPJ Web of Conferences **29**, 00035 (2012).
- [37] N. Zaim, A. Zaim, M. Kerouad, J. Alloys Compd. **663**, 516 (2016).
- [38] T. Kaneyoshi, Solid State Commun. **244**, 51 (2016).
- [39] A.E. Berkowitz, R.H. Kodama, S.A. Makhlof, F.T. Parker, F.E. Spada, E.J. McNiff Jr., S. Foner, J. Magn. Magn. Mater. **196-197**, 591 (1999).
- [40] W.H. Meiklejohn, C.P. Bean, Phys. Rev. **102**, 1413 (1956).
- [41] W.H. Meiklejohn, C.P. Bean, Phys. Rev. **105**, 904 (1957).
- [42] G.S.-Alvarez, J. Sort, S. Suriñach, M.D. Baró, J. Noguès, J. Am. Chem. Soc. **129**, 9102 (2007). **196**, 591 (1999).
- [43] M.E.J. Newman and G.T. Barkema, *Monte Carlo Methods in Statistical Physics* (Oxford University Press, New York, 1999).

- [44] D.P. Landau and K. Binder, *A Guide to Monte Carlo Simulations in Statistical Physics* (Cambridge University Press, Cambridge, U.K., 2000).
- [45] D.T. Robb, P.A. Rikvold, A. Berger, and M.A. Novotny, *Phys. Rev. E* **76**, 021124 (2007).
- [46] M. Acharyya, *Phys. Rev. E* **69**, 027105 (2004).
- [47] L. Néel, *Ann. Phys. Paris* **3**, 137 (1948).
- [48] J. Strečka, *Physica A* **360**, 379 (2006).
- [49] Ó. Iglesias, A. Labarta, and X. Battle, *J. Nanosci. Nanotechnol.* **8**, 6 (2008).
- [50] Y. Yüksel, E. Vatansever, and H. Polat, *J. Phys.: Condens. Matter* **24**, 436004 (2012).